Synthesis and photoluminescence of $Gd_2O_2S:Tb^{3+}$ nanoaggregates via one-pot solvothermal method

GUANGXI XU, HUA QIN*, TING HUANG, FAN LIU, JINGBAO LIAN
School of Mechanical Engineering, Liaoning Shihua University, P.R. China

Terbium ions doped gadolinium oxysulfide nanoaggregates have been successfully synthesized by one-pot solvothermal method. The undoped Gd_2O_2S show near-spherical structure with the diameter of ~400 nm. The XRD pattern shows pure hexagonal Gd_2O_2S phase can be obtained at 220 °C for 24 h. When the Gd_2O_2S doped with 7% Tb^{3+} ions, compared with the undoped samples, the phases at different temperature changed slightly, but the morphologies are greatly affected. Under ultraviolet (UV) light excitation, $Gd_2O_2S:Tb^{3+}$ nanoaggregates exhibit green emissions at 490 nm, 545 nm, 588 nm and 621 nm, corresponding to the $^5D_4 \rightarrow {}^7F_J$ (J=3, 4, 5 and 6) transitions of Tb^{3+} ions, respectively. The quenching concentration of Tb^{3+} ions is 3% with the longest fluorescent lifetime of t_1=162 μs and t_2=57514 μs.

(Received May 10, 2017; accepted November 28, 2017)

Keywords: Gadolinium oxysulfide, One-pot solvothermal method, Nanoaggregates, Luminescence properties

1. Introduction

In the last several decades, rare earth (RE) oxysulfides have aroused great attention due to their high chemical and thermal stability, high luminescence efficiency and unique physical properties [1,2], which have made them critically important for applying in catalyst, medical diagnostic imaging and luminescent host [3-5]. Recently, trivalent RE ions (Tb^{3+}, Eu^{3+} and Er^{3+}, etc) doped oxysulfides have become an important research hot topic among various phosphor materials. It is noted that terbium doped gadolinium oxysulfide ($Gd_2O_2S:Tb^{3+}$) phosphors which possess high density (≈7.34 g/cm^3), high melting point (2265 °C), lower excitation wavelength and short decay time [6,7] have been regarded as one of the most superior phosphors. Moreover, they can convert X-ray to visible light and exhibit green luminescence under the excitation of X-ray, cathode-ray or UV light [8]. Based on these properties, they have been widely applied in many fields, such as industrial inspection, flat-panel X-ray imaging, detector materials, luminescent sensors and inorganic light-emitting diodes [9-13].

For obtaining Gd_2O_2S samples, numerous synthetic approaches have been proposed, such as solid state method [14-18], precipitation method [19,20], combustion method [21], ELM method [22], solvothermal method [23], gas sulfuration method [24] etc, while these methods commonly involve higher reaction temperatures (nearly 1100 °C-1200 °C), conduct with complex processes and difficult to obtain perfect morphology [20,25,26]. Therefore, soft chemical methods have been gradually concerned, as they can successfully prepare RE oxysulfides with good morphologies and unique luminescence properties. While these methods are hard to realize, according to hard-soft acid-base theory (HSAB) [27], hard lewis acid and soft lewis base are difficult to bind to each other. Here, RE^{3+} belongs to hard lewis acid and S^{2-} belongs to soft lewis base, which lead to a low affinity between them [28]. For overcoming this shortcoming, thermolysis method has been reported [29,30], nevertheless, it still needs post annealing treatment to enhance the crystallinity and only can be used to prepare some middle RE oxysulfides. So, it is meaningful to find some other efficient ways to prepare the ideal products.

One-pot solvothermal method is one of the most promising techniques because of its advantages such as convenience route, friendly to the environment and easily to control the shapes [31,32]. In this regard, we adopted ethanediamine as the main solvent and sublimed sulfur powder as sulfur source, and by adjusting the temperature to 120 °C, 170 °C and 220 °C to investigate the effects of temperature on morphologies. Furthermore, the influence of terbium ions doped concentration on luminescence properties has also been discussed in detail.

2. Experiment

2.1. Materials and preparation

The gadolinium nitrate (99.99%), terbium nitrate (99.99%), sublimed sulfur powder, ethanediamine and absolute ethanol were used as starting materials without further purification. Ethanediamine was purchased from

Tianjin Zhiyuan Chemical Reagent Co. Ltd, China. Gadolinium nitrate and terbium nitrate were purchased from Jining Tianyi New Materials Co. Ltd, China. The other reagents were purchased from Sinopharm Chemical Reagent Co. Ltd, China. Firstly, the 0.2 M $Gd(NO_3)_3$ and $Tb(NO_3)_3$ ethanol solution (Solution 1) were prepared by dissolving the corresponding $Gd(NO_3)_3{\cdot}6H_2O$ and $Tb(NO_3)_3{\cdot}6H_2O$ in absolute ethanol. The ethylenediamine solution containing 10 mM sulfur (Solution 2) was prepared by dissolving a certain amount of sublimed sulfur powder in ethanediamine. With constant stirring, 5 ml Solution 1 was added dropwise into 65 mL Solution 2. The obtained suspension solution was transferred into a 100 mL para poly phenol (PPL) lined stainless steel autoclave and then heated in an electric blast drying oven for solvothermal reaction at different temperatures (120 °C, 170 °C and 220 °C) for 24 h. After cooled down to room temperature, the obtained sample was washed and centrifugated with absolute ethanol for several times and then dried overnight to get the final product. Through the same way, a series of Gd_2O_2S:$x$$Tb^{3+}$ samples were also prepared with different Tb^{3+} ions concentrations (x=1%, 3%, 5% and 7%).

2.2. Characterization measurements

FT-IR spectra were recorded in the region of 4000-400 cm^{-1} using a FT-IR-660+610 spectrophotometer by KBr method. To further analyze the structure of samples, D8Advance type diffractometer was used to recorded XRD patterns of samples at 40 kV and 100 mA with Co Kα(λ=1.789 Å) radiation. The morphologies of samples were analyzed by Hitachi SU8000 microscope operated at an acceleration voltage of 20 kV. The photoluminescence (PL) spectra and decay time were investigated using Hitachi F-7000 fluorescence spectrophotometer equipped with IBH tempro fluorescence lifetime measurement system. The CIE coordinates were calculated from the spectra based on the 1931 CIE standard for colorimetry.

3. Results and discussions

3.1. FT-IR spectra measurement

Fig. 1 shows the FT-IR spectra of Gd_2O_2S samples heated at 120 °C, 170 °C and 220 °C for 24 h, respectively. It can be seen from Fig. 1(a) that the absorption bands located at 3420 cm^{-1} and 1630 cm^{-1} are attributed to the stretching and bending vibrations of OH^- groups, arising from water molecules trapped by samples. Besides, the bands at 1510 cm^{-1}, 1400 cm^{-1}, 845 cm^{-1} and 740 cm^{-1} are attributed to the asymmetric splitting bending vibration of CO_3^{2-} groups, which formed on the surface of samples. With the temperature increased to 170 °C and 220 °C (Fig. 1(b) and Fig. 1(c)), the intensity of all of CO_3^{2-} and OH^- groups peaks decreased, suggesting the decreasing of gas adsorption ability (i.e. H_2O and CO_2) for the samples from Fig. 1(a) to (c). This result may be attributed to good crystallization of samples and diminishing surface defects with increasing synthetic temperature.

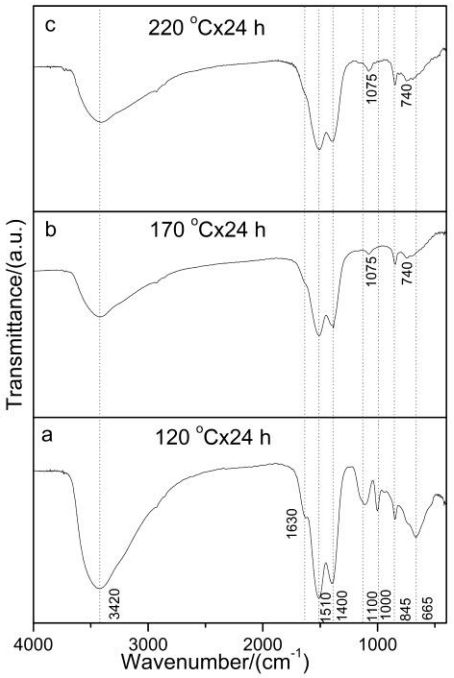

Fig. 1. FT-IR spectra of samples calcined at different temperatures for 24h: (a) 120 °C; (b) 170 °C; (c) 220 °C

3.2. XRD patterns measurement

To further investigate the effect of temperatures and doping on phase composition of the samples, the XRD patterns have been analyzed. Fig. 2 shows the XRD patterns of undoped and doped samples obtained at different temperatures for 24 h and the standard JCPDS:00-26-1422 of Gd_2O_2S phase. When the temperature amounts to 120 °C (Fig. 2(a)), the sample exhibits two board peaks around 2θ=29.35° and 46.58°, which indicates this solvothermal temperature is not sufficient to obtain a well crystallization. With the temperature increased to 170 °C (Fig. 2(c)), XRD pattern still remains amorphous, similar to Fig. 1(a). When the temperature increased to 220 °C (Fig. 2(e)), the samples have converted into hexagonal Gd_2O_2S phase, and all of the diffraction peaks are well matched with the JCPDS:00-26-1422 pattern, suggesting 220 °C is the suitable temperature to obtain the target product in this study. With the temperature varied from 120 °C to 220 °C, the peaks of samples become sharper, indicating the crystallinity of samples has been improved. Fig. 2(b), Fig. 2(d) and Fig. 2(f) show the samples doped with Tb^{3+} ions

(x=7%, consistent with the concentration of Fig. 4) at different temperatures. It can be seen that XRD patterns of doped samples barely appear peak shift. The reasons are as followed. As we all know, Gd^{3+} ions and Tb^{3+} ions have the similar ionic radii (Gd^{3+}=0.0938 nm, Tb^{3+}=0.0923 nm), so it is reasonable to believe that Tb^{3+} ions can dissolve into Gd_2O_2S lattice to occupy Gd^{3+} ions sites and keep the original phases composition [33].

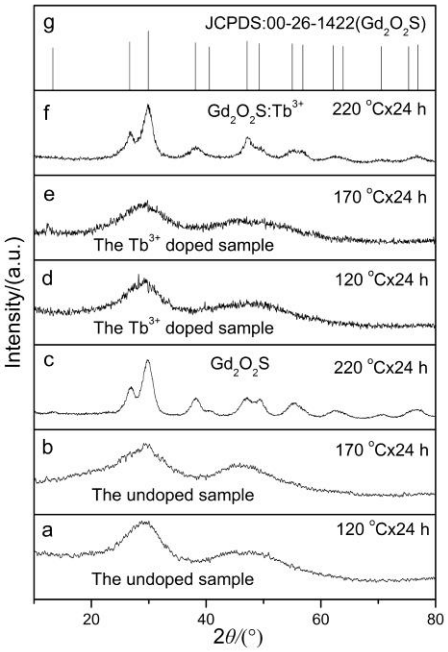

Fig. 2. XRD patterns of undoped and doped samples obtained at different temperatures for 24h as well as the standard card of Gd_2O_2S

Based on XRD patterns results, the phase formation process of Gd_2O_2S samples has been investigated. To best of our knowledge, Gd^{3+} ions are hard to bind to S^{2-} ions. In order to solve this problem, increasing the S reaction activity is an efficient way. Firstly, sulfur combined with ethanediamine and sulfur structure changed from ring to chain. Then, sulfur turned into sulfur polyanions with increasing temperature to 170 °C, but they are not stable at high temperature. Therefore, when the reaction temperature increased to 220 °C, sulfur polyanions were dissociated with S^{2-} ions, and the concentration of S^{2-} ions increased greatly, which improved the affinity between Gd^{3+} ions and S^{2-} ions and made them easier to combine [28,34].

3.3. SEM images measurement

Fig. 3 shows SEM images of the samples obtained at different reaction temperatures for 24 h. At 120 °C (Fig. 3(a)), the image shows a near-spherical structure with the diameter around 200 nm-300 nm, and the sample appears aggregation to some extend. When the temperature increased from 120 °C to 170 °C, the morphology of sample changed into flower-like with a hierarchical structure, consisting of many intercrossed nanosheets, and the average thickness is around 100 nm. When the temperature increased to 220 °C, the flower like structure disappeared and returned to near-spherical structure. The diameter increased to 400 nm and the degree of aggregation decreased. At the same time, the surface became more rougher than before. As we all know that the morphology of samples is influenced by many factors, including extrinsic (concentration of reagents) and intrinsic (temperature, pH). In this study, the changed morphologies of samples are arising from S^{2-} ions concentration. At 120 °C, sulfur structure changed from ring to chain, and few S^{2-} ions was produced. In this process, the morphology was influenced by ethidenediamine solvent, and obtained near-spherical Gd_2O_2S samples. With the temperature further increased, near-spherical samples were assembled and formed flower-like structure while the sulfur polyanions appeared, and little amount of S^{2-} ions released to some extend. Finally, at 220 °C, with the sulfur polyanions dissociated, many essential S^{2-} ions released. The number of nucleus become higher and the reunion speed of samples is faster than growth, which caused the petals ruptured and reassembled near-spherical structure with a lager size [28,35]. Through this principle, good crystallization samples have been successfully prepared.

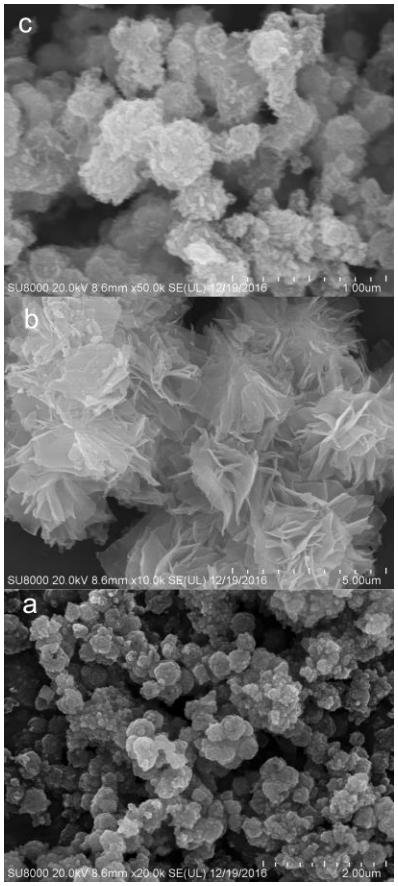

Fig. 3. SEM images of samples obtained at different temperatures for 24 h: (a) 120 °C; (b) 170 °C; (c) 220 °C

In order to figure out the effects of Tb^{3+} ions on Gd_2O_2S morphology, the doped samples at different temperatures have been shown in Fig. 4. It can be seen, at 120 °C, the morphology of doped samples is similar to the undoped one, when the temperature arrives at 170 °C, it still keeps the flower-like structure as Fig. 3(b), but the thickness of the intercrossed nanosheets has increased to some extend. When it reaches to 220 °C, the morphology has changed greatly from strips to small needles. It may be that as the temperature goes up, the effects of Tb^{3+} ions on the matrix has also increased. But, the certain reason still needs to be further investigated. Fig. 4(d) depicts EDX pattern of Gd_2O_2S doped with 7% Tb^{3+} ions. It shows that the concentration of Tb^{3+} ions is 6.77% in molar, indicating that Tb^{3+} ions are successfully doped into the samples. Besides, the elements concentration of Gd, Tb, O and S are 32.10%, 6.77%, 42.6% and 18.67%, respectively, which is close to the atomic ratio of 2:2:1 of $(Gd,Tb)_2O_2S$.

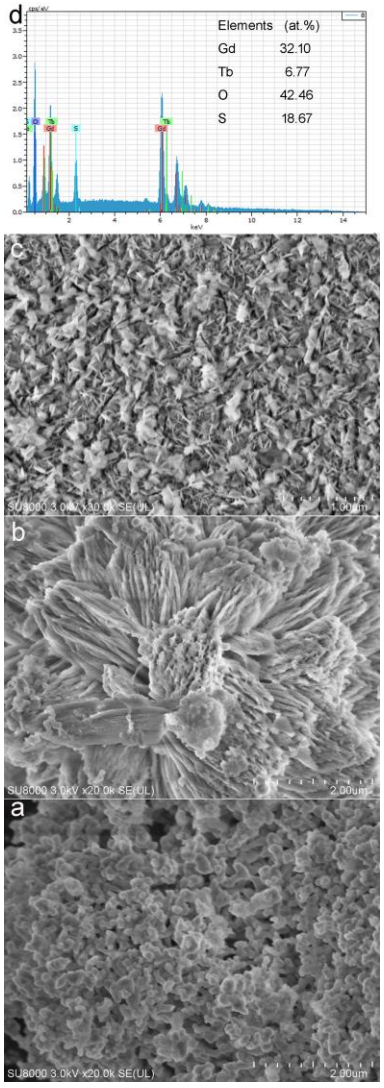

Fig. 4. SEM images of $Gd_2O_2S:Tb^{3+}$ samples obtained at different temperatures for 24 h: (a)120 °C; (b)170 °C; (c)220 °C and EDX spectrum (d) of $Gd_2O_2S:Tb^{3+}$ samples

3.4. PL spectra measurement

PL spectra of $Gd_2O_2S:xTb^{3+}$ (x=1%, 3%, 5% and 7%) nanoaggregates are shown in Fig. 5. The wavelength spectral ranges from 200 nm to 650 nm. In Fig. 5(a) shows a broad band absorption peak at 254 nm, which is attributed to 4f8→4f75d transition of Tb^{3+} ions. In Fig. 5(b) shows four narrow emission peaks at 490 nm, 545 nm, 588 nm and 621 nm, corresponding to $^5D_4 \rightarrow {}^7F_6$ (490 nm), $^5D_4 \rightarrow {}^7F_5$ (545 nm), $^5D_4 \rightarrow {}^7F_4$ (588 nm) and $^5D_4 \rightarrow {}^7F_3$(621 nm) transitions of Tb^{3+} ions, respectively.

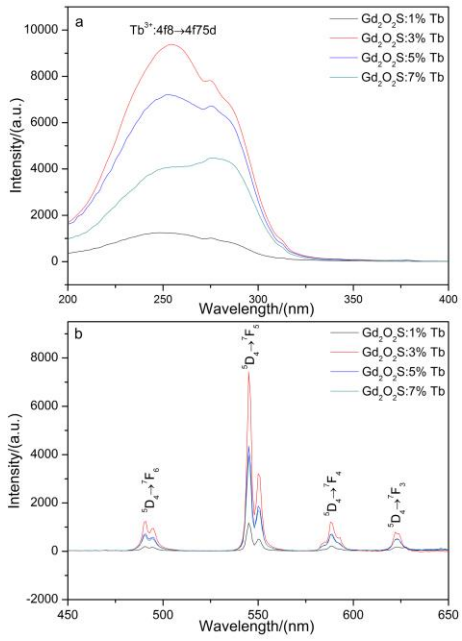

Fig. 5. PL spectra of $Gd_2O_2S:Tb^{3+}$ with different concentrations of Tb^{3+} ions

where 545 nm ($^5D_4 \rightarrow {}^7F_5$) shows the strongest green emission. This agrees well with the result reported by Yan et al. [36]. The emission intensity of $^5D_4 \rightarrow {}^7F_J$ increases with the increasing concentration of Tb^{3+} ions. Note that when x=3%, the luminous intensity reached the maximum value and then greatly decreased, as shown in Fig. 5(b). It indicates that 3% is the optimal doping concentration of Gd_2O_2S nanoaggregates. The main reason is ascribed to the concentration quenching of Tb^{3+} ions. With Tb^{3+} ions concentration increases, the distance between Tb^{3+} ions become smaller, which causes the non-radiative relaxation and weakened the luminous intensity [12].

3.5. Decay curves measurement

Fig. 6 shows decay curves of $Gd_2O_2S:xTb^{3+}$ (x=1%, 3%, 5% and 7%) nanoaggregates. These curves are fitted to the double exponential function:

$$I= I_0+Aexp(-t/\tau_1)+Bexp(-t/\tau_2) \quad (1)$$

where τ_1 and τ_2 represent the decay lifetime. In Fig. 6(a-d), the lifetimes of $Gd_2O_2S:Tb^{3+}$ nanoaggregates are 46 μs, 47624 μs; 162 μs, 57514 μs; 60 μs, 47152 μs and 58 μs, 658 μs, corresponding to the concentration of Tb^{3+} ions 1%, 3%, 5% and 7%, respectively. When the doping concentration of Tb^{3+} ions less than 3%, the decay time gradually became longer, once over 3%, it decreased greatly, which is well consistent to PL spectra analysis.

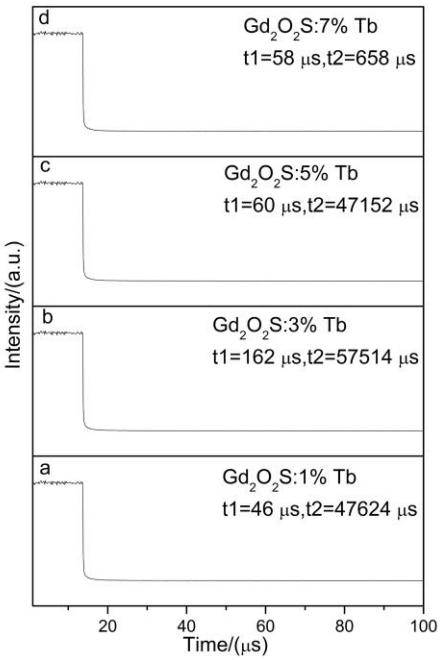

Fig. 6. Decay curves of $Gd_2O_2S:Tb^{3+}$ phosphors with different concentrations of Tb^{3+} ions: (a) x=1%; (b) x=3%; (c) x=5%; (d) x=7%

3.6. CIE chromaticity coordinate diagram

In order to figure out the emission color composition with different doping concentrations of Tb^{3+} ions, a CIE chromaticity coordinate diagram of $Gd_2O_2S:Tb^{3+}$ nanoaggregates have been presented in Fig. 7. From the CIE diagram it can be seen that with the concentration of Tb^{3+} ions increased, the CIE coordinate varied from (0.2946,0.5205) to (0.3109,0.5997), showing a brighter green emission. Besides, the tendency of *x* and *y* can nearly be seen as a linear decrease. Obviously, b (0.3109,0.5997) (*x*=3%) shows the purest green emission, and the green intensity gradually reduced when the concentration of Tb^{3+} ions is over 3%, which is also well consistent with PL spectra.

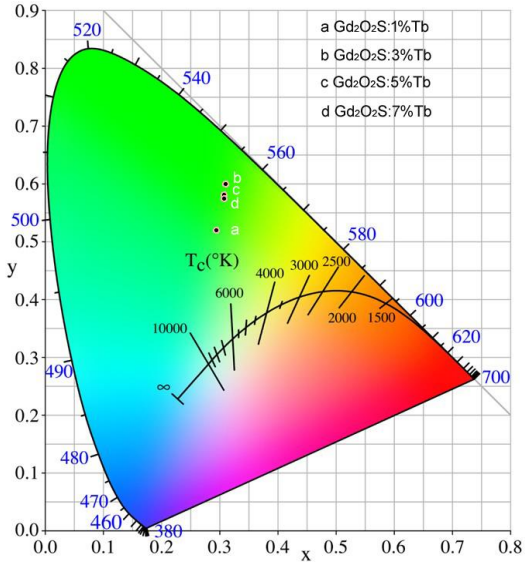

Fig. 7. CIE chromaticity coordinate diagram of $Gd_2O_2S:Tb^{3+}$ phosphors with different concentrations of Tb^{3+} ions: (a) x=1%; (b) x=3%; (c) x=5%; (d) x=7%

4. Conclusions

The hexagonal $Gd_2O_2S:Tb^{3+}$ nanoaggregates have been successfully developed by one-pot solvothermal method. The phase compositions and morphologies of samples are strongly dependent on the reaction temperature and the Tb^{3+} doping. With the reaction temperature amounts to 220 °C, pure Gd_2O_2S phase could be obtained and the as synthesized Gd_2O_2S nanoaggregates have near-spherical structure with the diameter of ~400 nm. When the samples doped with a certain amount of Tb^{3+} ions, the morphologies have changed as the temperature increases. Under UV light excitation, the $Gd_2O_2S:Tb^{3+}$ nanoaggregates exhibit strong green emission peaks at 545 nm, corresponding to $^5D_4 \rightarrow {}^7F_5$ transition of Tb^{3+} ions. The quenching concentration of Tb^{3+} ions is 3%, with the longest luminescence lifetime of t_1=162 μs and t_2=57514 μs corresponding to the CIE coordinate at (0.3109,0.5997).

Acknowledgments

This work was supported by National Student's platform for Innovation and Entrepreneurship Training Program (No.201710148000031) and Nature Science Foundation of Liaoning Province of China (No. 20170540582)

References

[1] M. Mikami, A, Oshiyama, Phys. Rev. B **57**(15), 8939 (1998).
[2] Bagheri Kh, Rezaee Ebrahim Saraee, H. R. Shakur, H.

Zamani Zeinali, Appl. Phys. A **122**, 1 (2016).
[3] X. Lu, L. Y. Yang, Q. L. Ma, J. Tian, X. G. Dong, Mater. Electron. **25**, 5388 (2014).
[4] K. Zhu, W. H. Ding, W. Sun, P. D. Han, L. X. Wang, Q. T. Zhang, Mater. Electron. **27**, 2379 (2016).
[5] W. Wang, Y. S. Li, H. M. Kou, S. P. Liu, W. P. Liu, Y. Shi, J. Li, X. Q. Feng, Y. B. Pan, J. K. Guo, Ceram. Technol. **42**, 199 (2015).
[6] K. R. Saraee, M. D. Zadeh, M. Mostajaboddavati, A. A. Kharieky, J. Electron. Mater. **45**(10), 4806 (2016).
[7] Y. J. Ding, Z. Y. Zhang, L. X. Wang, Q. T. Zhang, S. B. Pan, J. Mater. Sci.-Mater. El **28**(3), 2723 (2017).
[8] B. K. Cha, J. Y. Kim, T. J. Kim, C. Sim, G. Cho, Radiat. Meas. **45**(3-6), 742 (2010).
[9] A. A. da Silva, M. A. Lio Cebim, M. R. Davolos, J. Lumin. **128**(7), 1165 (2008).
[10] J. J. Dolo, O. M. Ntwaeaborwa, J. J. Terblans, E. Coetsee, B. F. Dejene, M. M. Biggs, H. C. Swart, Appl. Phys. A **101**(4), 655 (2010).
[11] G. Q. Wu, H. M. Qin, S. W. Feng, X. J. Tan, Z. H. Luo, Y. F. Liu, H. Z. Shao, J. Jiang, H. C. Jiang, Adv. Powder. Technol, **305**, 382 (2017).
[12] J. Silver, R. Withnall, Chem. Rev. **104**(6), 2833 (2004).
[13] J. Kido, Y. Okamoto, Chem. Rev. **102**(6), 2357 (2002).
[14] C. He, Z. G Xia, Q. L. Liu, Opt. Mater. **42**, 11 (2015).
[15] W. Fan, X. Y. Zhang, L. X. Chen, L. P. Lu, Crystengcomm. **17**(8), 1881 (2015).
[16] J. B. Lian, X. D. Sun, J. G Li, B. Xiao, K. Duan, Mater. Chem. Phys. **122**(2-3), 354 (2010) .
[17] J. W. Zhang, Y. L. Liu, S. Q. Man, J. Lumin. **117**(2), 141 (2006).
[18] S. Som, A. Choubey, S. K. Sharma, J. Exp. Nanosci. **10**(5), 350 (2015).
[19] F. Wang, B. Yang, X. M. Chen, W. H. Ma, B. Q. Xu, Mater. Chem. Phys. **169**, 113 (2016).
[20] A. Bagheri, K. R. E. Saraee, H. R. Shakur, H. Z. Zeinali, Appl. Phys. **122**, 553 (2016).
[21] S. S. Kang, J. K.Park, J. Y. Choi, B. Y. Cha, S. H. Cho, S. H. Nam, Nucl. Instrum. Meth. A **546**, 242 (2005).
[22] T. Hirai, T. Hirano, I. Komasawa, J. Coll. Int. Sci. **253**(1), 62 (2002).
[23] J. Huang, Y. H. Song, Y. Sheng, K. Y. Yan, H. B. Li, J. Alloy. Compd. **532**, 34 (2012).
[24] S. P. Mao, Q. Liu, M. Gu, D. L. Mao, C. K. Chang, J. Alloy. Compd. **465**(1-2), 367 (2008).
[25] Y. Tian, W. H. Cao, X. X. Luo, Y. Fu, J. Alloy. Compd. **433**(1-2), 313 (2007).
[26] A. M. Pires, O. A. Serra, M. R. Davolos, J. Lumin. **113**(3-4), 174 (2005).
[27] Y. Ding, J. Gu, J. Ke, Y. W. Zhang, C. H. Yan., Angewandte Chemie **50**(51), 12330 (2011).
[28] H. Liu, P. Liu, X. M. Su, J. Liu, X. Q. Li, H. D. Luo, Z. L. Yao, X. B. Yu, M. Zhan, RSC Adv. **4**, 57048 (2014).
[29] R. V. Rodrigues, L. C. Machado, J. R. Matos, E. J. B. Muri, A. A. L. Marins, H. F. Brito, C. A. C. Passos, J. Therm. Anal. Calorim. **122**(2), 765 (2015).
[30] M. Leskelä, L. Niinistö, Anal. Calorim. **18**(2), 307 (1980).
[31] J. Thirumalai, R. Chandramohan, T. A. Vijayan, Mater. Electron. **22**(8), 936 (2011).
[32] J. Liu, H. D. Luo, P. J. Liu, L. X. Han, X. Zheng, B. Xu, X. B. Yu, Dalton Trans. **41**(45), 13984 (2012).
[33] R. D. Shannon, Acta Cryst. A **32**, 751 (1976).
[34] D. K. Ma, S. S. Liu, Y. Q. Zhang, C. W. Zhang, S. M. Huang, J. Exp. Nanosci. **8**(4), 434 (2013).
[35] X. M. Zhang, J. Wang, K. Guo, H. H. Chen, X. X. Yang, J. T. Zhao, J. Alloy. Compd. **517**, 149 (2014).
[36] X. Yan, G R. Fern, R. Withnall, J. Silver, Nanoscale **5**(18), 8640 (2013).

*Corresponding author: huaqin1978@163.com